IOPscience iopscience.iop.org

Home Search Collections Journals About Contact us My IOPscience

Magnetic properties of the $S = 1/2$ distorted diamond chain at $T = 0$

This article has been downloaded from IOPscience. Please scroll down to see the full text article.

2003 J. Phys.: Condens. Matter 15 5979

(http://iopscience.iop.org/0953-8984/15/35/307)

View the table of contents for this issue, or go to the journal homepage for more

Download details:
IP Address: 171.66.16.125
The article was downloaded on 19/05/2010 at 15:08

Please note that terms and conditions apply.

INSTITUTE OF PHYSICS PUBLISHING JOURNAL OF PHYSICS: CONDENSED MATTER

J. Phys.: Condens. Matter **15** (2003) 5979–5995 PII: S0953-8984(03)63153-X

Magnetic properties of the $S = 1/2$ distorted diamond chain at $T = 0$

Kiyomi Okamoto[1], **Takashi Tonegawa**[2] **and Makoto Kaburagi**[3]

[1] Department of Physics, Tokyo Institute of Technology, Oh-Okayama, Meguro-ku, Tokyo 152-8551, Japan
[2] Department of Mechanical Engineering, Fukui University of Technology, Gakuen 3-Chome, Fukui-Shi 910-8505, Japan
[3] Faculty of Cross-Cultural Studies, Kobe University, Tsurukabuto, Nada-ku, Kobe 657-8501, Japan

Received 2 May 2003
Published 22 August 2003
Online at stacks.iop.org/JPhysCM/15/5979

Abstract

We explore, at $T = 0$, the magnetic properties of the $S = 1/2$ antiferromagnetic distorted diamond chain described by the Hamiltonian $\mathcal{H} = \sum_{j=1}^{N/3}\{J_1(\boldsymbol{S}_{3j-1}\cdot\boldsymbol{S}_{3j} + \boldsymbol{S}_{3j}\cdot\boldsymbol{S}_{3j+1}) + J_2\boldsymbol{S}_{3j+1}\cdot\boldsymbol{S}_{3j+2} + J_3(\boldsymbol{S}_{3j-2}\cdot\boldsymbol{S}_{3j} + \boldsymbol{S}_{3j}\cdot\boldsymbol{S}_{3j+2})\} - H\sum_{l=1}^{N} S_l^z$ with J_1, J_2, $J_3 \geqslant 0$, which models well $A_3Cu_3(PO_4)_4$ with A = Ca, Sr, $Bi_4Cu_3V_2O_{14}$ and azurite $Cu_3(OH)_2(CO_3)_2$. We employ the physical consideration, degenerate perturbation theory, level spectroscopy analysis of the numerical diagonalization data obtained by the Lanczos method and also the density matrix renormalization group (DMRG) method. We investigate the mechanisms of the magnetization plateaux at $M = M_s/3$ and $(2/3)M_s$, and also show the precise phase diagrams of the $(J_2/J_1, J_3/J_1)$ plane concerned with these magnetization plateaux, where $M = \sum_{l=1}^{N} S_l^z$ and M_s is the saturation magnetization. We also calculate the magnetization curves and the magnetization phase diagrams by means of the DMRG method.

1. Introduction

Low-dimensional quantum spin systems have attracted increasing attention in recent years. A few years ago, Ishii *et al* [1] reported the experimental results on a trimerized $S = 1/2$ quantum spin chain $Cu_3Cl_6(H_2O)_2{\cdot}2H_8C_4SO_2$. From the structural analysis experiment they proposed a model, shown in figure 1, for this substance [1]. The Hamiltonian of this model is written as

$$\mathcal{H} = \mathcal{H}_0 + \mathcal{H}_Z \tag{1}$$

 © 2003 IOP Publishing Ltd Printed in the UK

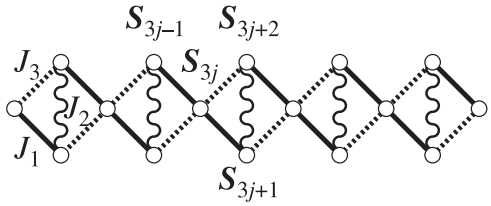

Figure 1. Sketch of the DD chain. Full lines denote the coupling J_1, wavy lines the coupling J_2 and dotted lines the coupling J_3. We can assume $J_1 \geqslant J_3$ without loss of generality.

$$\mathcal{H}_0 = J_1 \sum_{j=1}^{N/3} (\boldsymbol{S}_{3j-1} \cdot \boldsymbol{S}_{3j} + \boldsymbol{S}_{3j} \cdot \boldsymbol{S}_{3j+1}) + J_2 \sum_{j=1}^{N/3} \boldsymbol{S}_{3j+1} \cdot \boldsymbol{S}_{3j+2} + J_3 \sum_{j=1}^{N/3} (\boldsymbol{S}_{3j-2} \cdot \boldsymbol{S}_{3j} + \boldsymbol{S}_{3j} \cdot \boldsymbol{S}_{3j+2}) \tag{2}$$

$$\mathcal{H}_Z = -H \sum_{l=1}^{N} S_l^z \tag{3}$$

where $\boldsymbol{S}_l$ is the $S = 1/2$ operator at the lth site and N is the total number of spins in the system. All the coupling constants, J_1, J_2 and J_3, are supposed to be positive (antiferromagnetic). Hereafter we set $\tilde{J}_2 \equiv J_2/J_1$ and $\tilde{J}_3 \equiv J_3/J_1$. The magnetic field is denoted by H. We can assume $J_1 \geqslant J_3$ without loss of generality because the $J_1 < J_3$ case is equivalent to the $J_1 > J_3$ case by interchanging the roles of J_1 and J_3.

This model has been named the 'distorted diamond (DD) chain model' [2]. The name 'diamond' comes from the suit in playing cards, and 'distorted' from the fact that $J_1 \neq J_3$ in general. The symmetric case ($J_1 = J_3$) had first been proposed by Takano, Kubo and Sakamoto (TKS) [3] earlier than Ishii *et al* [1] and ourselves [2]. We [2] have investigated the ground state properties of the $S = 1/2$ DD chain model when $H = 0$ by an analytical method as well as by level spectroscopy (LS) analysis of the numerical diagonalization data obtained by the Lanczos technique. Later theoretical studies on the $S = 1/2$ DD chain were also reported by ourselves [4, 5], Sano and Takano [6] and Honecker and Läuchli [7].

Unfortunately the substance which was thought to be $Cu_3Cl_6(H_2O)_2{\cdot}2H_8C_4SO_2$ at first [1] has been proven to be $Cu_2Cl_4{\cdot}H_8C_4SO_2$, the lattice of which has been shown to be the two-leg zig-zag chain with bond alternation by the same group [8]. Now, however, the $S = 1/2$ DD chain model is again in the spotlight as a model for $A_3Cu_3(PO_4)_4$ with A = Ca, Sr [9–11], $Bi_4Cu_3V_2O_{14}$ [12] and azurite $Cu_3(OH)_2(CO_3)_2$.

For $A_3Cu_3(PO_4)_4$ with A = Ca, Sr, Drillon *et al* [9, 10] measured the magnetic susceptibility $\chi(T)$, the specific heat $C(T)$ and the magnetization process $M(H)$, and proposed the model without J_2 interactions. Ajiro *et al* [11] performed a high field magnetization process measurement up to 40 T and a neutron diffraction experiment, and proposed a model with J_2 interactions. In these reports, a wide magnetization plateau at $M = M_s/3$ was observed, where M is the z component of the total spin, defined by $M = \sum_{l=1}^{N} S_l^z$, and M_s is the saturation magnetization. The behaviour of $\chi(T)$ and neutron diffraction results suggest that these substances are ferrimagnetic (FRI) above the three-dimensional ordering temperature.

Sakurai *et al* [12] reported $\chi(T)$, $M(H)$ (up to 28 T), $C(T)$ and the ^{51}V NMR of $Bi_4Cu_3V_2O_{14}$. Unfortunately, they could not reach any conclusion on the existence of the

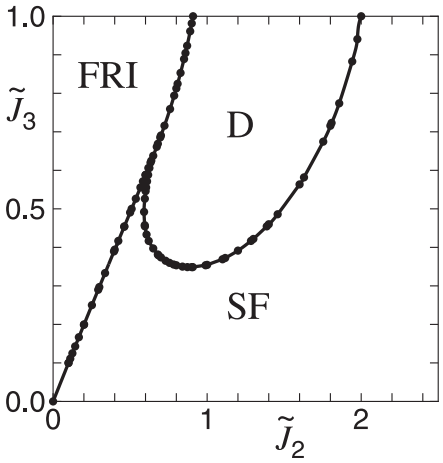

Figure 2. Zero-field ground state phase diagram of the $S = 1/2$ DD chain model. The $\tilde{J}_3 = 1$ case is reduced to the model of TKS [3]. There are three phases in this phase diagram; the FRI phase, the D phase and the SF phase. The TD and DM states found by TKS [3] are realized on the $\tilde{J}_3 = 1$ line in the D and SF regions, respectively.

$M = M_s/3$ plateau because $M \sim 0.27M_s$ even when $H = 28$ T. The FRI behaviour was not seen in $\chi(T)$ above the three-dimensional ordering temperature. It seems that this substance has a spin-fluid (SF) ground state above the three-dimensional ordering temperature.

Very recently, Kikuchi and co-workers [13–15] have reported experimental results on the magnetic and thermal properties of azurite $Cu_3(OH)_2(CO_3)_2$. Following their reports, azurite has a SF ground state and a wide magnetization plateau at $M = M_s/3$.

Thus, above the three-dimensional ordering temperature, the ground states of $A_3Cu_3(PO_4)_4$ with A = Ca, Sr seem to be FRI, whereas those of $Bi_4Cu_3V_2O_{14}$ and azurite $Cu_3(OH)_2(CO_3)_2$ seem to be SF. In view of these situations, we think it is very important to investigate the magnetic properties of the $S = 1/2$ DD chain model in more detail. Throughout this paper we consider the $T = 0$ case.

This paper is organized as follows. The ground-state properties at zero magnetic field are reviewed in section 2. The magnetization plateaux at $M = M_s/3$ and $(2/3)M_s$ are discussed in sections 3 and 4, respectively. The numerical results for the magnetization curves and the magnetization phase diagram are presented in section 5. The last section 6 is devoted to a discussion and summary.

2. Review of the ground-state properties at zero magnetic field

Discussions presented in this section are confined to the case where $H = 0$. We [2] have investigated the ground state of the $S = 1/2$ DD chain model by an analytical method as well as the LS analysis of the numerical diagonalization data obtained by the Lanczos technique, and obtained the phase diagram shown in figure 2. There are three phases in this phase diagram; the FRI phase, the dimer (D) phase and the SF phase. The magnitude S_{tot} of the total spin $\boldsymbol{S}_{tot}$, defined by $\boldsymbol{S}_{tot} \equiv \sum_{l=1}^{N} \boldsymbol{S}_l$ and $\boldsymbol{S}_{tot}^2 = S_{tot}(S_{tot} + 1)$, is $S_{tot} = N/6$ in the FRI phase, whereas $S_{tot} = 0$ in the D and SF phases. In the D phase, there is a finite energy gap between the doubly degenerate ground state and the first excited state, while in the SF phase there is no energy gap.

When $J_2 = 0$, we can readily know that the ground state is the FRI state with $S_{tot} = N/6$ by use of the Lieb–Mattis theorem [16]. The physical pictures of the FRI state are shown

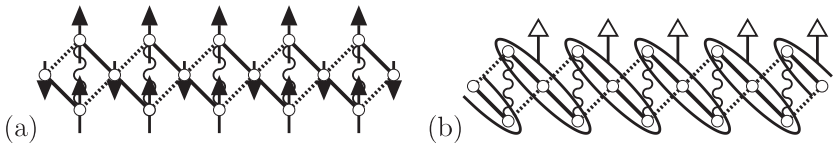

Figure 3. Physical pictures of the FRI ground state for the $S = 1/2$ DD chain model. Open ellipses with open triangles in (b) denote the three-spin clusters in the state ϕ_1.

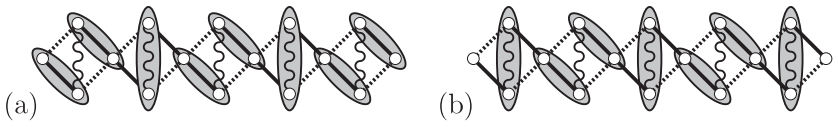

Figure 4. Physical pictures of the D ground state for the $S = 1/2$ DD chain model. Two spins in a shadowed ellipse effectively form a singlet D pair.

in figure 3, where part (a) holds good for the $J_1 \sim J_3$ case, whereas (b) holds good for the $J_1 \gg J_2$, J_3 case. The ellipses in (b) denote the effective three-spin cluster which is formed when the interaction J_1 is much larger than the interactions J_2 and J_3. We represent the $S_l^z = 1/2$ and $-1/2$ states of the lth single spin by $\uparrow_l$ and $\downarrow_l$, respectively. Then, the ground state wavefunctions of the jth cluster in the case of $J_2 = J_3 = 0$ are expressed as

$$\phi_{1,j} = \frac{1}{\sqrt{6}}(|\uparrow_{3j-1}\uparrow_{3j}\downarrow_{3j+1}\rangle - 2|\uparrow_{3j-1}\downarrow_{3j}\uparrow_{3j+1}\rangle + |\downarrow_{3j-1}\uparrow_{3j}\uparrow_{3j+1}\rangle) \tag{4}$$

and

$$\phi_{2,j} = \frac{1}{\sqrt{6}}(|\downarrow_{3j-1}\downarrow_{3j}\uparrow_{3j+1}\rangle - 2|\downarrow_{3j-1}\uparrow_{3j}\downarrow_{3j+1}\rangle + |\uparrow_{3j-1}\downarrow_{3j}\downarrow_{3j+1}\rangle) \tag{5}$$

for $S_{\rm tot}^{(3)z} = 1/2$ and $-1/2$, respectively, where $S_{\rm tot}^{(3)z}$ is the z component of the total spin of the three-spin cluster. When all the three-spin clusters are effectively in the ϕ_1 (or ϕ_2) state, the FRI state shown by figure 3(b) is realized. This physical consideration has been developed in [4, 7] by use of degenerate perturbation theory [17] around the point $\tilde{J}_2 = \tilde{J}_3 = 0$. In fact, the quantum phase transition between the FRI and SF phases takes place at $\tilde{J}_3 = \tilde{J}_2$ near $(\tilde{J}_2, \tilde{J}_3) = (0, 0)$, and it is of the first order. This shows very good agreement with the numerical results (see figure 2). The quantum phase transition between the FRI and D phases is also of the first order.

In the case of $J_3 = 0$, our DD chain is reduced to the J_1–J_1–J_2 trimerized antiferromagnetic chain, the ground state of which is the SF state. In particular, in the case of $J_1 = J_2$, it is further simplified to the uniform antiferromagnetic chain.

The D phase is caused by the frustration, and is doubly degenerate due to the spontaneous breaking of the translational symmetry (SBTS), as shown in figure 4. The D phase is realized in the region where the frustration effect seems to be severe. We note that there is no frustration when $J_2 = 0$ or $J_3 = 0$. The quantum phase transition between the SF and D phases is essentially the same as that in the $S = 1/2$ chain with next-nearest-neighbour interactions [18, 19], and is of the Berezinskii–Kosterlitz–Thouless (BKT) type [20, 21], as has been fully discussed in our previous paper [2].

As we have mentioned in section 1, the symmetric case $J_1 = J_3$, which is shown in figure 5(a), has first been proposed by TKS [3]. They found that the ground state is one of the following three states: the FRI state, the tetramer–dimer (TD) state or the dimer–monomer (DM) state, depending on whether $\tilde{J}_2 < 0.909, 0.909 < \tilde{J}_2 < 2$ or $2 < \tilde{J}_2$. The value

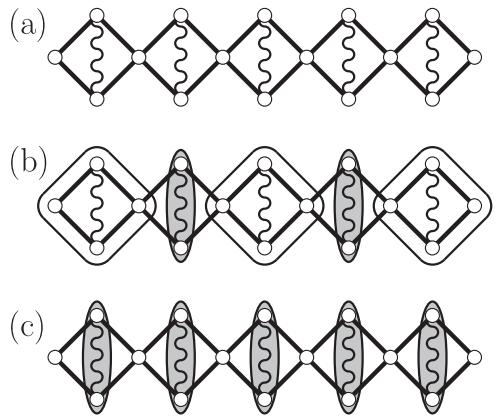

Figure 5. (a) The model of TKS [3]. (b) The TD state, where the rectangles represent tetramers and the ellipses singlet Ds. (c) The DM state.

0.909 of the FRI–TD boundary has been calculated by the numerical method, whereas the value 2 of the TD–DM boundary is the exact one obtained by an analytical method. In the TD state, as shown in figure 5(b), four spins of the diamond unit $\boldsymbol{S}_{3j-3}$, $\boldsymbol{S}_{3j-2}$, $\boldsymbol{S}_{3j-1}$ and $\boldsymbol{S}_{3j}$ (or $\boldsymbol{S}_{3j}$, $\boldsymbol{S}_{3j+1}$, $\boldsymbol{S}_{3j+2}$ and $\boldsymbol{S}_{3j+3}$) form a tetramer, and two spins $\boldsymbol{S}_{3j+1}$ and $\boldsymbol{S}_{3j+2}$ (or $\boldsymbol{S}_{3j+4}$ and $\boldsymbol{S}_{3j+5}$) form a singlet D. Obviously, the TD state is doubly degenerate due to the SBTS. In the DM state, on the other hand, two spins $\boldsymbol{S}_{3j+1}$ and $\boldsymbol{S}_{3j+2}$, connected by the J_2 interactions, form a singlet D and the remaining joint spins $\boldsymbol{S}_{3j}$ are completely free, as shown in figure 5(c). Thus, the DM state is $2^{N/3}$-fold degenerate. It is very interesting that the ground state can be exactly expressed as the direct product of the local states in a finite range of the parameter region $\tilde{J}_2 > 0.909$.

The TD state is very peculiar to the $J_1 = J_3$ case. Namely, if $J_1 > J_3$, the tetramer which consists of $\boldsymbol{S}_{3j-3}$, $\boldsymbol{S}_{3j-2}$, $\boldsymbol{S}_{3j-1}$ and $\boldsymbol{S}_{3j}$ is effectively decomposed into two Ds, the ($\boldsymbol{S}_{3j-3}$, $\boldsymbol{S}_{3j-2}$) pair and the ($\boldsymbol{S}_{3j-1}$, $\boldsymbol{S}_{3j}$) pair. Two spins in each pair are connected by the J_1 interaction, which is larger than the J_3 one. This decomposition leads to the doubly degenerate D state shown in figure 4. Thus, the TD state is the special case of the doubly degenerate D state.

The $2^{N/3}$-fold degeneracy of the DM state is lifted when $J_1 \neq J_3$. In other words, the effective interaction between the free spins $\boldsymbol{S}_{3j}$ and $\boldsymbol{S}_{3(j+1)}$ appears through the D located between them. Honecker and Läuchli [7] have derived the effective interaction between $\boldsymbol{S}_{3j}$ and $\boldsymbol{S}_{3(j+1)}$ as

$$J_{\mathrm{eff}} = \frac{(J_1 - J_3)^2}{J_2}\left(\frac{1}{2} + \cdots\right) \tag{6}$$

which leads to the SF ground state. The effective interaction J_{eff} vanishes when $J_1 = J_3$, which is consistent with TKS's result [3] on the DM state. Then, the DM state is also peculiar to the $J_1 = J_3$ case and is the special case of the SF state.

3. Magnetization plateau at $M = M_{\mathrm{s}}/3$

In this section, we discuss the magnetization plateau at $M = M_{\mathrm{s}}/3$. Since the Hamiltonian has the trimer nature, as is shown in figure 6, the mechanism for the $M = M_{\mathrm{s}}/3$ plateau is just the same as that for the trimerized chain (figure 7) investigated by Okamoto and Kitazawa [22] and Honecker [23]. The $M = M_{\mathrm{s}}/3$ plateau can be realized without any SBTS. This is

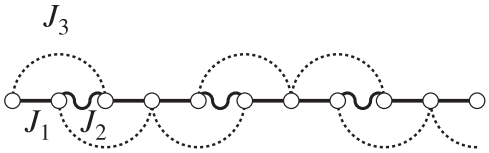

Figure 6. Single-chain representation of the DD chain model.

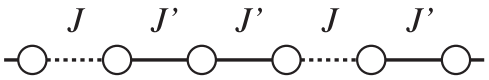

Figure 7. Antiferromagnetic chain with the trimerization.

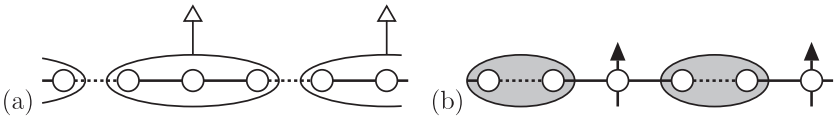

Figure 8. Two mechanisms for the $M = M_s/3$ plateau for the $S = 1/2$ trimerized chain: (a) plateau A and (b) plateau B. Open ellipses denote the trimers with $S_{tot}^{(3)z} = 1/2$ and shaded ellipses denote the singlet Ds.

consistent with the necessary condition for the magnetization plateau by Oshikawa, Yamanaka and Affleck (OYA) [24]:

$$n(S - \langle m \rangle) = \text{integer} \tag{7}$$

where n is the periodicity of the wavefunction of the plateau state, S is the magnitude of the spins and $\langle m \rangle$ is the average magnetization per one spin in the plateau.

Here we explain the mechanism for the $M = M_s/3$ plateau of the $S = 1/2$ trimerized chain. When $0 < J \ll J'$, each of three spins connected by J' forms an effective trimer with $S_{tot}^{(3)z} = 1/2$ (or $-1/2$), the wavefunction of which is ϕ_1 (or ϕ_2). When the magnetic field is applied, all the trimers belong to the $S_{tot}^{(3)z} = 1/2$ state, which brings about $M = M_s/3$, as shown in figure 8(a). The plateau due to this mechanism is named 'plateau A'. The mechanism of the plateau A state is essentially the same as that of the FRI state for the $J_1 \gg J_2$, J_3 case when $H = 0$, which has already been explained in section 2. When $J \gg J' > 0$, on the other hand, each pair of two spins connected by J forms an effective singlet D pair and the remaining spins are nearly free. When the magnetic field is applied, the nearly free spins turn in the direction of the field, resulting also in $M = M_s/3$, as shown in figure 8(b). We call the plateau due to this mechanism 'plateau B'. Thus, there are two mechanisms for the $M = M_s/3$ plateau. It is easily seen that the change of the plateau mechanism occurs at $J = J'$, where the trimerized chain is reduced to the uniform chain having no gap (i.e. no plateau) in the excitation spectrum. This situation is most simply seen in the trimerized XY chain [25] which is exactly solvable.

A similar situation is expected to hold for the present $S = 1/2$ DD chain model. The pictures of plateaux A and B are depicted in figures 9(a) and (b), respectively, by use of the diamond form. When $J_3 = 0$, our model is reduced to the simple trimerized chain discussed above. Then, the change of the plateau mechanism occurs at $J_1 = J_2$ when $J_3 = 0$. To find the phase boundary between plateaux A and B for the general case, we have to rely on the numerical method. One of the most powerful methods is the LS [26, 27] method. Kitazawa [28] has developed the LS for this kind of transition (belonging to the Gaussian

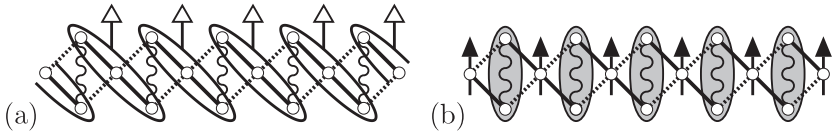

Figure 9. Two mechanisms for the $M = M_s/3$ plateau for the $S = 1/2$ DD chain: (a) plateau A and (b) plateau B. Shaded ellipses denote the singlet Ds and open ellipses denote the trimers with $S^{(3)z}_{\rm tot} = 1/2$.

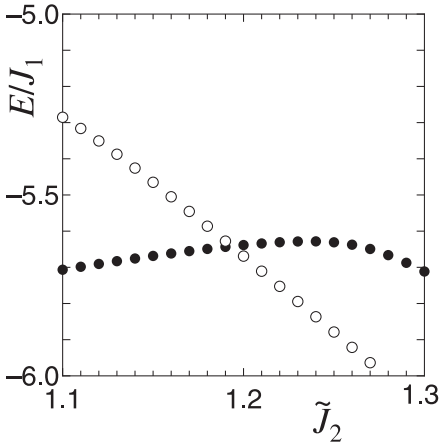

Figure 10. Crossing of the lowest energies in the $M = M_s/3$ sector with $P = 1$ (full circles) and $P = -1$ (open circles) for the $N = 18$ and $\tilde{J}_3 = 0.55$ cases under the TBC, when $\tilde{J}_2$ is run. The crossing point of these two curves is located at $\tilde{J}_2 \simeq 1.193$.

universality class) by use of the twisted boundary condition (TBC) instead of the periodic boundary condition (PBC). This method has been applied to several magnetization plateau problems in a successful way [22, 29–31].

In finite size systems with the PBC, the $M = M_s/3$ plateau state changes smoothly from the plateau A state to the plateau B state when the parameter J_2/J_1 runs from 0 to ∞, although the plateau width takes the smallest value at the transition point. Under the TBC

$$\boldsymbol{S}_N \cdot \boldsymbol{S}_1 \Rightarrow -S^x_N S^x_1 - S^y_N S^y_1 + S^z_N S^z_1, \tag{8}$$

on the other hand, the plateau A state and the plateau B state can be easily distinguished, even in finite size systems, by the eigenvalue P of the space inversion operator

$$\boldsymbol{S}_j \Rightarrow \boldsymbol{S}_{N-j+1}. \tag{9}$$

Since it is believed that the boundary condition does not affect any physical quantities in the $N \to \infty$ limit, we distinguish the ground state by comparing the lowest energies with $P = \pm 1$. In other words, we can find the phase boundary between plateaux A and B from the crossing of the lowest energies with $P = \pm 1$ as functions of the quantum parameters in the Hamiltonian. This is the physical interpretation of Kitazawa's TBC method [28]. He [28] has consolidated the foundations of his TBC method by use of bosonization, renormalization group method and conformal field theory.

Figure 10 shows the crossing of the lowest energies with $P = \pm 1$ when $N = 18$ and $\tilde{J}_3 = 0.55$. We can see that two curves cross each other at $\tilde{J}^{(\rm cr)}_2(18) \simeq 1.193$, close to which the quantum transition point $\tilde{J}^{(\rm cr)}_2$ between the plateau A and B phases for the $N \to \infty$ system is

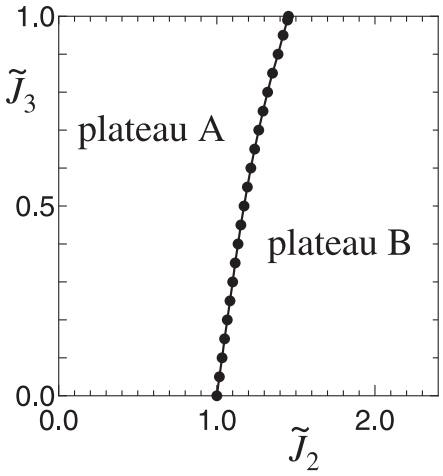

Figure 11. $M = M_s/3$ plateau phase diagram of the $S = 1/2$ DD chain model.

expected to be located. An accurate value of $\tilde{J}_2^{(cr)}$ may be estimated by extrapolating $\tilde{J}_2^{(cr)}(N)$ to the $N \to \infty$ limit. Performing this extrapolation we have assumed an N dependence of $\tilde{J}_2^{(cr)}(N)$ as

$$\tilde{J}_2^{(cr)}(N) = \tilde{J}_2^{(cr)} + c_1/N^2 + c_2/N^4 \tag{10}$$

where c_1 and c_2 are numerical constants, and have employed the finite size values, $\tilde{J}_2^{(cr)}(12)$, $\tilde{J}_2^{(cr)}(18)$ and $\tilde{J}_2^{(cr)}(24)$. Repeating this procedure with sweeping $\tilde{J}_3$, we have obtained the $M = M_s/3$ plateau phase diagram shown in figure 11. The estimated value of errors of the phase boundary is, for instance, $\tilde{J}_2^{(cr)} = 1.193 \pm 0.001$ (or better) for $\tilde{J}_3 = 0.55$.

We have performed the density matrix renormalization group (DMRG) calculation [32, 33] to obtain the ground state magnetization curves and the magnetization phase diagrams for our $S = 1/2$ DD chain model, the details of which will be described in section 5. Here, we present in figure 12 the width $W_{(1/3)}$ (see equation (29) below) of the $M = M_s/3$ plateau for $\tilde{J}_3 = 0.55$ in the $N \to \infty$ limit; in this figure $W_{(1/3)}$ is plotted as a function of $\tilde{J}_2$. The point where $W_{(1/3)}$ vanishes is the transition point ($\tilde{J}_2 \simeq 1.193$), the result shown in figure 12 being in very good agreement with the above-mentioned result obtained by the LS method with the TBC. We see a cusp in the curve at $\tilde{J}_2 \simeq 0.561$. This cusp corresponds to the FRI–SF transition in figure 2 (see also figure 19(b)). In fact, an infinitesimally small field brings about the $M = M_s/3$ magnetization state in the FRI region, whereas a finite field is required for the $M = M_s/3$ magnetization state in the SF and D regions.

Let us now discuss the expectation value $\langle S_l^z \rangle$ of each spin in the $M = M_s/3$ plateau state. In the plateau A region, the approximate wavefunction of the jth three-spin cluster is

$$\phi_{1,j} = \frac{1}{\sqrt{6}}(|\uparrow_{3j-1}\uparrow_{3j}\downarrow_{3j+1}\rangle - 2|\uparrow_{3j-1}\downarrow_{3j}\uparrow_{3j+1}\rangle + |\downarrow_{3j-1}\uparrow_{3j}\uparrow_{3j+1}\rangle) \tag{11}$$

which leads to

$$\langle S_{3j-1}^z \rangle = \langle S_{3j+1}^z \rangle = \tfrac{1}{3} \qquad \langle S_{3j} \rangle = -\tfrac{1}{6}. \tag{12}$$

Thus, the expectation values $\langle S_l^z \rangle$ should be

$$\left\{\ldots, \left(\tfrac{1}{3}, -\tfrac{1}{6}, \tfrac{1}{3}\right), \left(\tfrac{1}{3}, -\tfrac{1}{6}, \tfrac{1}{3}\right), \left(\tfrac{1}{3}, -\tfrac{1}{6}, \tfrac{1}{3}\right), \ldots\right\} \tag{13}$$

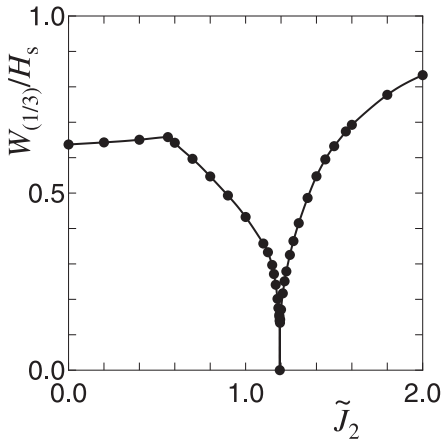

Figure 12. Normalized $M = M_s/3$ plateau width $W_{(1/3)}/H_s$ as a function of $\tilde{J}_2$ when $\tilde{J}_2 = 0.55$, where H_s is the saturation field. The plateau width $W_{(1/3)}$ vanishes at $\tilde{J}_3 \simeq 1.193$, which well agrees with the transition point between plateaux A and B in figure 11. The cusp at $\tilde{J}_3 \simeq 0.561$ corresponds to the FRI–SF transition in figure 2.

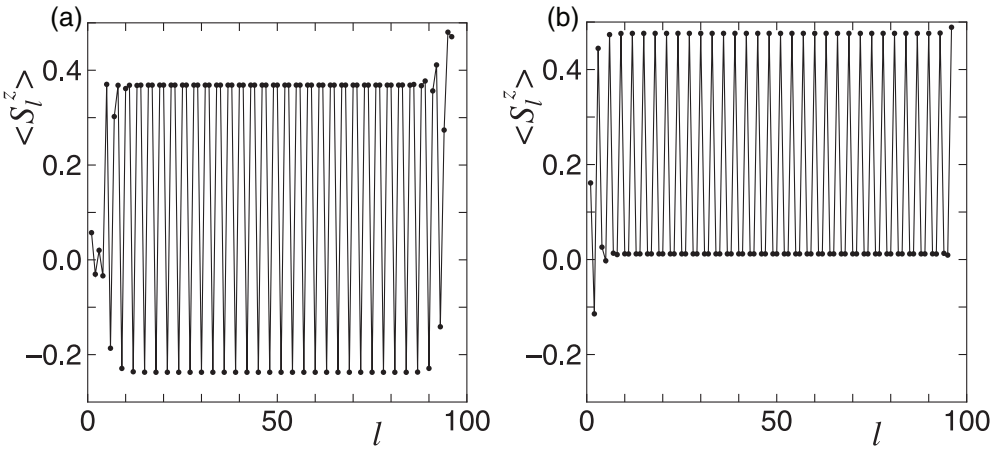

Figure 13. Behaviour of $\langle S_l^z \rangle$ of the $N = 96$ system (a) in the plateau A region, where $(\tilde{J}_2, \tilde{J}_3) = (0.80, 0.55)$, and (b) in the plateau B region, where $(\tilde{J}_2, \tilde{J}_3) = (1.50, 0.55)$.

where three spins in a parenthesis form a three-spin cluster. In the plateau B region, on the other hand, it is very easy to see that $\langle S_l^z \rangle$ should be

$$\left\{\ldots, (0,0), \tfrac{1}{2}, (0,0), \tfrac{1}{2}, (0,0), \tfrac{1}{2}, (0,0), \tfrac{1}{2}, \ldots\right\} \tag{14}$$

where two spins in a parenthesis form a singlet D. Figure 13 shows the DMRG result for $\langle S_l^z \rangle$ for the $N = 96$ system in the plateau A region, where $(\tilde{J}_2, \tilde{J}_3) = (0.80, 0.55)$, and that in the plateau B region, where $(\tilde{J}_2, \tilde{J}_3) = (1.50, 0.55)$. Then, the behaviour of $\langle S_l^z \rangle$ in this figure is quite consistent with our picture of the mechanisms for the $M = M_s/3$ plateau.

4. Magnetization plateau at $M = (2/3)M_s$

Our incipient discussions on the $M = (2/3)M_s$ plateau of the $S = 1/2$ DD chain model are given in a previous paper [5]; here we aim at discussing it in much more detail.

Since the unit cell of the present model consists of three $S = 1/2$ spins, the OYA condition [24] tells us that, if the SBTS does not occur, the possible magnetization plateau for $0 < M < M_s$ is only at $M = M_s/3$. Thus, the SBTS is necessary for the realization of the $M = (2/3)M_s$ plateau. In the three-spin cluster limit where $\tilde{J}_2 = \tilde{J}_3 = 0$, the $M = (2/3)M_s$ magnetization state is realized when half of the three-spin clusters are in the $S_{tot}^{(3)z} = 1/2$ state and the remaining half are in the $S_{tot}^{(3)z} = 3/2$ state. The configuration of these two states is completely free when $\tilde{J}_2 = \tilde{J}_3 = 0$, resulting in the $2^{N/3}$-fold degeneracy. This high degeneracy is lifted when we introduce $\tilde{J}_2$ and $\tilde{J}_3$.

Let us discuss the $M = (2/3)M_s$ magnetization plateau problem based on the above picture by use of the degenerate perturbation theory [17]. The lowest energy state of the jth three-spin cluster with $S_{tot}^{(3)z} = 1/2$ is given by

$$\psi_{1,j} = \frac{1}{\sqrt{6}}(|\uparrow_{3j-1}\uparrow_{3j}\downarrow_{3j+1}\rangle - 2|\uparrow_{3j-1}\downarrow_{3j}\uparrow_{3j+1}\rangle + |\downarrow_{3j-1}\uparrow_{3j}\uparrow_{3j+1}\rangle) \tag{15}$$

which is nothing other than equation (4). Here we use the symbol $\psi_{1,j}$ for convenience. The energy of this state is

$$E_1 = -J_1 - \tfrac{1}{2}H. \tag{16}$$

On the other hand, the state of the jth three-spin cluster with $S_{tot}^{(3)z} = 3/2$ is

$$\psi_{2,j} = |\uparrow_{3j-1}\uparrow_{3j}\uparrow_{3j+1}\rangle \tag{17}$$

having the energy

$$E_2 = \tfrac{1}{2}J_1 - \tfrac{3}{2}H. \tag{18}$$

Using the pseudo-spin operator $\boldsymbol{T}_j$, where $\boldsymbol{T}_j^2 = T_j(T_j + 1)$ with $T_j = 1/2$, we express the $\psi_{1,j}$ and $\psi_{2,j}$ states by the $T_j^z = -1/2$ and $+1/2$ states, respectively. We neglect the other six states of the jth three-spin cluster, which can be justified near $\tilde{J}_2 = \tilde{J}_3 = 0$. We note that $E_1 = E_2$ when the magnetic field is given by $H = H_{2/3}^{(0)} \equiv (3/2)J_1$. The lowest-order perturbation calculation with respect to $\tilde{J}_2$ and $\tilde{J}_3$ leads to the effective Hamiltonian for the pseudo-spin operator $\boldsymbol{T}_j$

$$\mathcal{H}_{eff} = \sum_j \{J_{eff}^{\perp}(T_j^x T_{j+1}^x + T_j^y T_{j+1}^y) + J_{eff}^z T_j^z T_{j+1}^z\} - H_{eff}\sum_j T_j^z \tag{19}$$

where

$$J_{eff}^{\perp} = \frac{J_2 - 4J_3}{6} \tag{20}$$

$$J_{eff}^{z} = \frac{J_2 + 8J_3}{36} \tag{21}$$

$$H_{eff} = H - H_{2/3}^{(0)} - \frac{5J_2 + 22J_3}{36}. \tag{22}$$

The ground state of the effective Hamiltonian (19) is either the Néel state or the SF state, depending on whether $\Delta_{eff} > 1$ or $0 \leqslant \Delta_{eff} \leqslant 1$, where Δ_{eff} is

$$\Delta_{eff} \equiv \frac{J_{eff}^z}{|J_{eff}^{\perp}|} = \frac{J_2 + 8J_3}{6|J_2 - 4J_3|}. \tag{23}$$

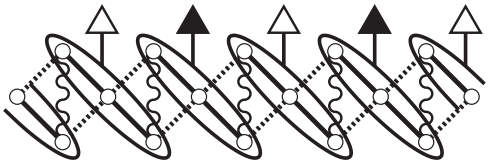

Figure 14. Physical picture of the $M = (2/3)M_s$ plateau state for the $S = 1/2$ DD chain model. Ellipses with open and full triangles denote the three-spin clusters with the ψ_1 and ψ_2 states, respectively.

Thus, the Néel ground state is realized when

$$\frac{5}{32} < \frac{J_3}{J_2} < \frac{7}{16}. \tag{24}$$

The Néel and SF ground states in the $\boldsymbol{T}$ picture correspond to the $M = (2/3)M_s$ plateau-full and plateau-less states in the original $\boldsymbol{S}$ picture, respectively. The transition between the plateau-full and plateau-less states is of the BKT type [20, 21]. The magnetic field $H_{2/3}$ given by the solution of $H_{\rm eff} = 0$, i.e.

$$H_{2/3} \equiv H_{2/3}^{(0)} + \frac{5J_2 + 22J_3}{36} = \frac{54J_1 + 5J_2 + 22J_3}{36} \tag{25}$$

represents the magnetic field corresponding to the centre of the magnetization plateau in the plateau-full case, and that corresponding to the $M = M_s/3$ magnetization in the plateau-less case. This degenerate perturbation calculation has already been developed in [5, 7]. The physical picture of the $M = (2/3)M_s$ plateau is shown in figure 14.

For the purpose of drawing the $M = (2/3)M_s$ plateau phase diagram, we have performed the numerical diagonalization of the finite size Hamiltonian by the Lanczos method. We can apply the LS method [19, 26, 27, 34, 35] to this kind of plateau-full–plateau-less transition of the BKT type [36–39] accompanied by the SBTS. The plateau-full–plateau-less transition point can be obtained from the crossing point of $\Delta E_0(N, M = (2/3)M_s)$ and $\Delta E_{\pm 1}(N, M = (2/3)M_s)$ as functions of the quantum parameters. Here, $\Delta E_0(N, M)$ and $\Delta E_{\pm 1}(N, M)$ are defined, respectively, by

$$\Delta E_0(N, M) \equiv E_1(N, M) - E_0(N, M) \tag{26}$$

$$\Delta E_{\pm 1}(N, M) \equiv \tfrac{1}{2}\{E_0(N, M + 1) + E_0(N, M - 1)\} - E_0(N, M) \tag{27}$$

where $E_0(N, M)$ and $E_1(N, M)$ are, respectively, the lowest and second lowest energies in the subspace of the magnetization M for the finite size system with N spins. It is noted that the $M = (2/3)M_s$ state is either plateau-full (the Néel state in the $\boldsymbol{T}$ picture) or plateau-less (the SF state in the $\boldsymbol{T}$ picture), depending on whether $\Delta E_0(N, M = (2/3)M_s) < \Delta E_{\pm 1}(N, M = (2/3)M_s)$ or $\Delta E_0(N, M = (2/3)M_s) > \Delta E_{\pm 1}(N, M = (2/3)M_s)$.

Figure 15 shows the behaviours of $\Delta E_0(N, M = (2/3)M_s)$ and $\Delta E_{\pm 1}(N, M = (2/3)M_s)$ with $N = 18$ ($M_s = 9$) as functions of $\tilde{J}_3$ when $\tilde{J}_2 = 0.80$. The value of $\tilde{J}_3$ at each crossing point is expected to be an approximate value for the plateau-full–plateau-less transition point $\tilde{J}_3^{(\rm cr)}$ in the $N \to \infty$ limit. We have carried out, to estimate $\tilde{J}_3^{(\rm cr)}$, an extrapolation to this limit similar to that in the case of the estimation of $\tilde{J}_2^{(\rm cr)}$ for the $M = M_s/3$ plateau phase diagram, discussed in section 3, and have obtained the $M = (2/3)M_s$ plateau phase diagram depicted in figure 16. In this figure a good agreement is found between the numerical result and the analytical prediction given by equation (24) near $(\tilde{J}_2, \tilde{J}_3) = (0, 0)$. We note that the point $\Delta E_0 = 0$ ($\tilde{J}_3 \simeq 0.25$) corresponds to the Ising case ($J_{\rm eff}^{\perp} = 0$) of the pseudo-spin Hamiltonian (19). The double degeneracy in the Néel ground state is realized only in the

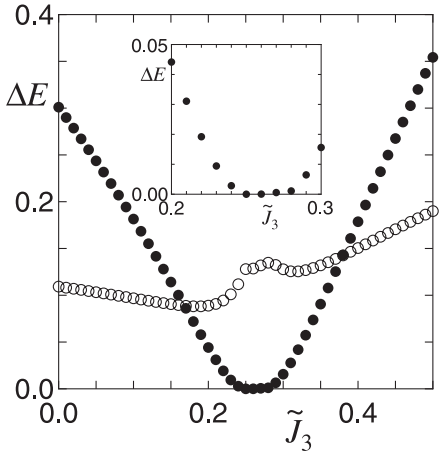

Figure 15. $\Delta E_0(N, M = (2/3)M_s)$ (full circles) and $\Delta E_{\pm 1}(N, M = (2/3)M_s)$ (open circles) with $N = 18$ ($M_s = 9$) as functions of $\tilde{J}_3$ when $\tilde{J}_2 = 0.80$. Approximate values for the plateau-full–plateau-less phase boundary points in the $N \to \infty$ limit are known from the crossings of $\Delta E_0(N, M = (2/3)M_s)$ and $\Delta E_{\pm 1}(N, M = (2/3)M_s)$. The point where $\Delta E_0(N, M = (2/3)M_s)$ vanishes ($\tilde{J}_3 \simeq 0.25$; see the inset) corresponds to the Ising case of the pseudo-spin Hamiltonian (19).

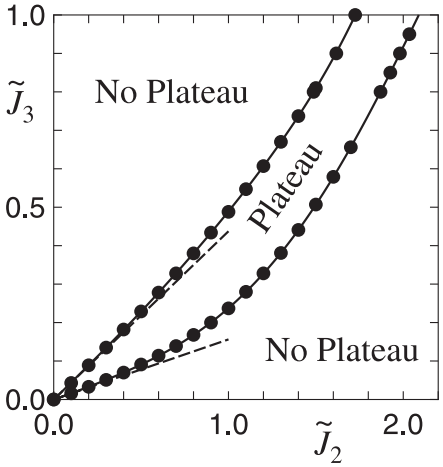

Figure 16. $M = (2/3)M_s$ plateau phase diagram of the $S = 1/2$ DD chain model. Full circles denote the numerical results and the broken lines the results of the degenerate perturbation calculation given by equation (24).

$N \to \infty$ limit in the usual cases, whereas it is realized even in finite size systems for the Ising case. Thus, the point $\Delta E_0 = 0$, which means the doubly degenerate ground state, corresponds to the Ising case.

The expectation value $\langle S_l^z \rangle$ of the $(2/3)M_s$ plateau state can be obtained from the above-mentioned physical picture (figure 14): equations (15) and (17) yield for $\langle S_l^z \rangle$

$$\left\{ \ldots, \overbrace{\left(\tfrac{1}{3}, -\tfrac{1}{6}, \tfrac{1}{3}\right)}^{\psi_1}, \overbrace{\left(\tfrac{1}{2}, \tfrac{1}{2}, \tfrac{1}{2}\right)}^{\psi_2}, \overbrace{\left(\tfrac{1}{3}, -\tfrac{1}{6}, \tfrac{1}{3}\right)}^{\psi_1}, \overbrace{\left(\tfrac{1}{2}, \tfrac{1}{2}, \tfrac{1}{2}\right)}^{\psi_2}, \ldots \right\} \tag{28}$$

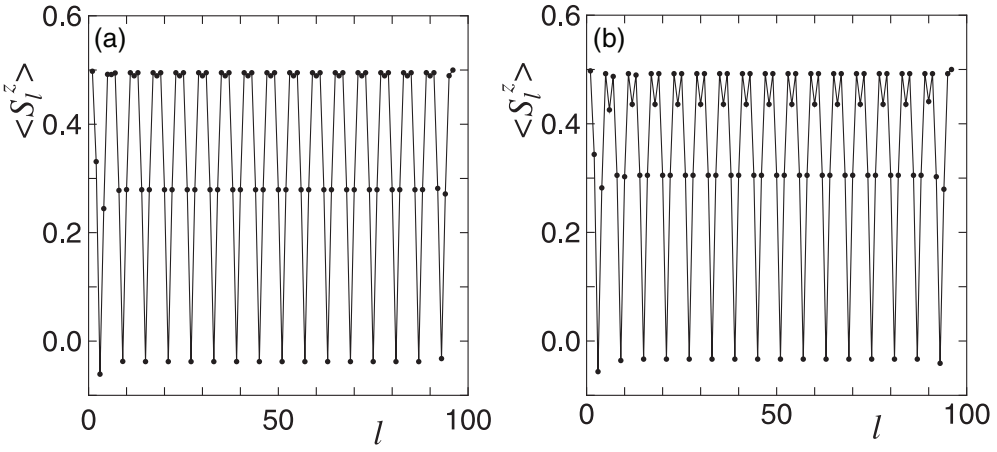

Figure 17. Behaviour of $\langle S_l^z \rangle$ of the $N = 96$ system in the $M = (2/3)M_s$ plateau state, where (a) $(\tilde{J}_2, \tilde{J}_3) = (0.80, 0.27)$ and (b) $(\tilde{J}_2, \tilde{J}_3) = (0.80, 0.30)$.

where three spins in a parenthesis form a three-spin cluster. Figure 17 shows the behaviours of $\langle S_l^z \rangle$ which are obtained by using the DMRG method for the $N = 96$ system in the $(\tilde{J}_2, \tilde{J}_3) = (0.80, 0.27)$ and $(0.80, 0.30)$ cases. As can be readily seen, the behaviour of $\langle S_l^z \rangle$ is quite consistent with equation (28). Of course, the ideal behaviour given by this equation is expected in the $\Delta_{\rm eff} = \infty$ limit (the Ising limit) in the effective Hamiltonian (19), even if the mapping onto the $\boldsymbol{T}$ picture is justified. In the case where $\Delta_{\rm eff}$ is finite, the hybridization between the ψ_1 and ψ_2 states occurs, which well explains the fact that $\langle S_{3j}^z \rangle < \langle S_{3j-1}^z \rangle = \langle S_{3j+1}^z \rangle$ in the ψ_2-rich cluster. The behaviour of $\langle S_l^z \rangle$ of the ψ_2-rich cluster in the $(\tilde{J}_2, \tilde{J}_3) = (0.80, 0.27)$ case is nearer to the ideal behaviour than that in the $(\tilde{J}_2, \tilde{J}_3) = (0.80, 0.30)$ case. This suggests that the parameter set in the former case is nearer to the Ising limit of the effective Hamiltonian (19) than that in the latter case. In fact, the Ising limit is realized when $\tilde{J}_3 \simeq 0.25$ for $\tilde{J}_2 = 0.55$, as can be seen from figure 15.

5. Magnetization curves and magnetization phase diagrams

In order to calculate the ground state magnetization curve of the present $S = 1/2$ DD chain model, we have employed the DMRG method [32, 33]. The procedure of our DMRG calculation is briefly summarized in [4].

We have computed $E_0(N, M)$ for finite size systems with up to $N = 96$ ($N = 216$) spins for general (special) values of $\tilde{J}_2$ and $\tilde{J}_3$. Once the values of $E_0(N, M)$ for all nonnegative M's ($M = 0, 1, 2, \ldots, N/2$) are known, the ground state magnetization curve can be obtained by plotting as a function of H the average magnetization $\langle m \rangle$ per one spin, where $\langle m \rangle$ is the value of m which yields the minimum among $\{E_0(N, mN)/N - Hm\}$'s with $m = 0, 1/N, 2/N, \ldots, 1/2$. As is naturally expected, the resulting magnetization curve is a stepwise increasing function of H. Following Bonner and Fisher's pioneering work [40], we may obtain, except for plateau regions, a satisfactorily good approximation to the ground state magnetization curve in the $N \to \infty$ limit by drawing a smooth curve through the midpoints of the steps in the finite size results. As for the plateau regions, on the other hand, we can estimate the lowest and highest values of H in the $N \to \infty$ limit, denoted by $H_{\rm p,l}$ and $H_{\rm p,h}$, respectively,

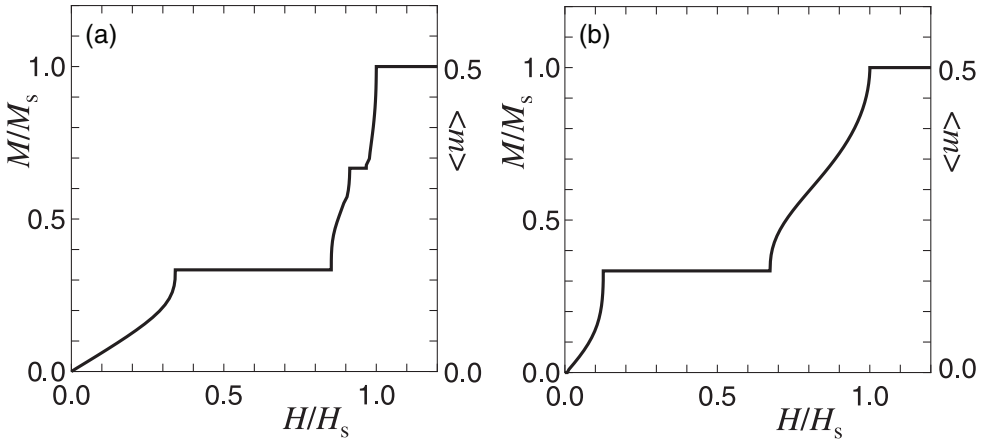

Figure 18. Magnetization curves in the $N \to \infty$ limit for (a) $(\tilde{J}_2, \tilde{J}_3) = (0.80, 0.27)$ and (b) $(\tilde{J}_2, \tilde{J}_3) = (0.80, 0.55)$. Note that H_s denotes the saturation field. The wide plateau at $M = M_s/3$ is observed in both (a) and (b). The $M = (2/3)M_s$ plateau can be seen in (a), the parameters for which lie in the plateau region shown in figure 16.

giving the $M = pM_s$ ($p = 0$, $1/3$, $2/3$ or 1) plateau by extrapolating the corresponding finite size values to this limit.

The magnetization curves in the $N \to \infty$ limit thus obtained for the $(\tilde{J}_2, \tilde{J}_3) = (0.80, 0.27)$ case and the $(\tilde{J}_2, \tilde{J}_3) = (0.80, 0.55)$ case are shown in figure 18. It is noted that $H_{p,l}$ and $H_{p,h}$ in both cases are estimated by fitting the finite size results for $N = 48$, 72 and 96 to a quadratic function of $1/N^2$, which is similar to equation (10). The $H = 0$ ground state phase in the former case is the SF phase (see figure 2), and therefore we have no $M = 0$ plateau. Since that in the latter case is the D phase, on the other hand, we have in principle a finite $M = 0$ plateau, although the $M = 0$ plateau width is so narrow that we cannot see it clearly (see figure 19(b)). The wide $M = M_s/3$ plateaux are found in both cases, while the $M = (2/3)M_s$ plateau is observed only in the former case, which is consistent with the $M = (2/3)M_s$ plateau phase diagram shown in figure 16.

We have also obtained the magnetization phase diagrams on the $(\tilde{J}_3, H)$ plane for the case of $\tilde{J}_2 = 0.80$ and on the $(\tilde{J}_2, H)$ plane for the case of $\tilde{J}_3 = 0.55$. The results are depicted in figure 19, where $H_{0,h}/H_s$, $H_{1/3,l}/H_s$, $H_{1/3,h}/H_s$, $H_{2/3,l}/H_s$ and $H_{2/3,h}/H_s$ as well as $H/H_s = 1.0$, where H_s ($\equiv H_{1,l}$) is the saturation field, are plotted. When we estimate these values for general values of $\tilde{J}_2$ and $\tilde{J}_3$, we have employed the same method as that for the estimations of $\tilde{J}_2^{(cr)}$ in section 3 and $\tilde{J}_3^{(cr)}$ in section 4. It should be emphasized, however, that in estimating $H_{1/3,l}$ and $H_{1/3,h}$ for special values of $\tilde{J}_2 = 1.190$, 1.191, 1.192, 1.194 and 1.195 with $\tilde{J}_3 = 0.55$, we have used the finite size results for $N = 132$, 168 and 216 instead of those for $N = 48$, 72 and 96, since the N dependence of the finite size results are rather strong for these $\tilde{J}_2$ and $\tilde{J}_3$. In the case of $\tilde{J}_2 = 0.80$ the change of the mechanism of the $M = M_s/3$ plateau is not observed, whereas in the case of $\tilde{J}_3 = 0.55$, it is clearly observed. This is quite consistent with the $M = M_s/3$ plateau phase diagram shown in figure 16. We note that, in the case of $\tilde{J}_3 = 0.55$, the $M = M_s/3$ plateau starts from $H = 0$ when $0 \leqslant \tilde{J}_2 < 0.561$, since the $H = 0$ ground state phase is the FRI phase. Finally, we mention that the $M = M_s/3$ plateau width $W_{(1/3)}$ plotted in figure 12 is defined by

$$W_{(1/3)} = H_{1/3,h} - H_{1/3,l}. \tag{29}$$

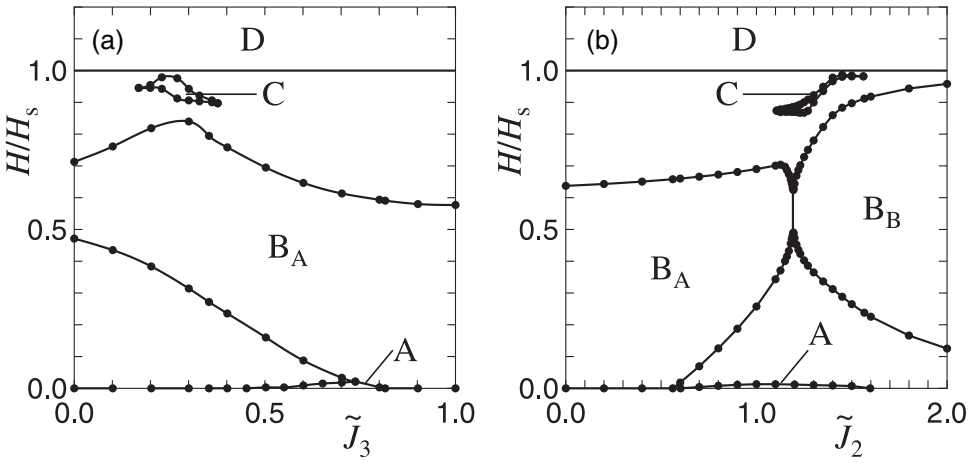

Figure 19. Magnetization phase diagrams (a) on the H/H_s versus $\tilde{J}_3$ plane when $\tilde{J}_2 = 0.80$ and (b) on the H/H_s versus $\tilde{J}_2$ plane when $\tilde{J}_3 = 0.55$. In the regions A, B_X (X = A, B), C and D, the average magnetization $\langle m \rangle$ per one spin is equal to zero (the $M = 0$ plateau region), 1/6 (the $M = M_s/3$ plateau region), 1/3 (the $M = (2/3)M_s$ plateau region) and 1 (the $M = M_s$ plateau, or the saturated magnetization, region), respectively; the B_A and B_B regions are, respectively, for the plateaux A and B. In the other regions, $\langle m \rangle$ varies continuously with the increase of H. For (b), we can see the closing of the $M = M_s/3$ plateau at $\tilde{J}_2 = 1.193$, which corresponds to the phase transition between the plateau A and B phases, as expected from the $M = M_s/3$ phase diagram shown in figure 11. For (a), such a transition is not seen, which is also consistent with the $M = M_s/3$ phase diagram.

6. Discussion and summary

We have investigated the magnetic properties of the $S = 1/2$ DD chain model at $T = 0$ by use of degenerate perturbation theory, LS analysis of the numerical diagonalization data obtained by the Lanczos method, and DMRG calculations. We have clarified the mechanism for the $M = M_s/3$ and $(2/3)M_s$ plateaux, and have also drawn the precise plateau phase diagrams by carrying out the LS analysis. These phase diagrams agree with the results obtained by physical considerations and the degenerate perturbation theory. The expectation value $\langle S_l^z \rangle$ of each spin estimated by the DMRG calculation strongly supports the plateau formation mechanisms. The magnetization curves for a few sets of the parameters $\tilde{J}_2$ and $\tilde{J}_3$ have been obtained by the DMRG calculation, the behaviour of which are consistent with the plateau phase diagrams. We have also drawn the magnetization phase diagram on the $(\tilde{J}_3, H)$ plane for $\tilde{J}_2 = 0.80$ and that on the $(\tilde{J}_2, H)$ plane for $\tilde{J}_3 = 0.55$.

As noted in section 1, some substances are thought to be well modelled by the DD chain. $A_3Cu_3(PO_4)_4$ with A = Ca, Sr were investigated by Drillon *et al* [9, 10] and Ajiro *et al* [11]. The measured magnetic susceptibility $\chi(T)$ [9, 10] showed the FRI behaviour. In the high field magnetization process measurement by Ajiro *et al* [11], the magnetization rapidly reached the wide $M = M_s/3$ plateau as the magnetic field was increased. The $M = M_s/3$ plateau was kept even at the high field limit 40 T in their experiment. Ajiro *et al* [11] performed the neutron scattering experiment for $Sr_3Cu_3(PO_4)_4$ at $T = 4$ K and 70 mK. The transition temperature of the three-dimensional ordering to the antiferromagnetic state of $Sr_3Cu_3(PO_4)_4$ is $T_N = 0.96$ K. Although their neutron diffraction pattern at $T = 70$ mK was consistent with the antiferromagnetic ordering, its magnitude was strongly reduced to almost 1/10 of that in the usual cases. This fact suggests that the magnitude of spins on average is about $1/\sqrt{10} \sim 1/3$

of that for independent spins, which is consistent with the picture of the three-spin cluster formation with $S_{\rm tot}^{(3)z} = \pm 1/2$. Thus, we think, the parameter set of this substance lies in the FRI region on the phase diagram figure 2.

Sakurai *et al* [12] investigated the magnetic susceptibility, magnetization process (up to 28 T) and ^{51}V NMR of $Bi_4Cu_3V_2O_{14}$. Unfortunately, they could not obtain any conclusion on the existence of the $M = M_{\rm s}/3$ plateau, because $M \simeq 0.27M_{\rm s}$ at $H = 28$ T. This suggests that the ground state of this substance above the three-dimensional antiferromagnetic ordering temperature ($T_{\rm N} = 6$ K) is the SF state. The FRI behaviour was not seen in the susceptibility above $T_{\rm N}$, which is consistent with the SF ground state.

Kikuchi *et al* [13–15] have investigated experimentally the magnetic and thermal properties of azurite $Cu_3(OH)_2(CO_3)_2$, which seems to be modelled by the $S = 1/2$ DD chain model. Their result [13] shows that the $H = 0$ ground state of azurite is the SF state. Furthermore, their recent result [15] for the low temperature magnetization curve obtained by applying the magnetic field along the b axis (the chain axis) demonstrates that the $M = M_{\rm s}/3$ plateau appears in the field range of $0.5H_{\rm s} \lesssim H \lesssim 0.8H_{\rm s}$ with $H_{\rm s} \sim 32.5$ T. These two results may imply that $\tilde{J}_3$ is considerably smaller than unity and $\tilde{J}_2$ is considerably larger than unity, as can be seen from figure 2, since the $M = M_{\rm s}/3$ plateau width should be much wider if $\tilde{J}_3 \sim 1$ and $\tilde{J}_2 \gtrsim 2$. It is noted that the fact that $\tilde{J}_3$ is smaller than unity is not inconsistent with the fact [41] that the length of the bond between the $(3j-1)$th and $(3j)$th sites is almost equal to that of the bond between the $(3j)$th and $(3j+1)$th sites, since the superexchange paths connecting $\boldsymbol{S}_{3j-1}$ and $\boldsymbol{S}_{3j}$ and that connecting $\boldsymbol{S}_{3j}$ and $\boldsymbol{S}_{3j+1}$ are different to each other. Thus, we conjecture that the $M = M_{\rm s}/3$ plateau observed in azurite is the plateau B shown in figure 9(b) (see figure 11). In addition to the above experimental results, Kikuchi and Mitsudo [15] have also found a plateau-like behaviour at $M = (2/3)M_{\rm s}$ in the $\mathrm{d}M/\mathrm{d}H$ versus H curve. This may suggest that the value of $\tilde{J}_2$ is not so much larger compared with unity (see figure 16). Furthermore, they [15] have observed the anisotropy concerning the direction of the applied magnetic field in the low temperature magnetization curves. Thus, in order to quantitatively explain the magnetic properties of azurite, more detailed investigations, which take at least the antisymmetric Dzyaloshinsky–Moriya interactions [42, 43] into account, are definitely required. We, however, believe that we have succeeded in explaining them at least qualitatively.

The specific heat measurement of azurite has also been done by Kikuchi and Mitsudo [15]. They have found two peaks in the specific heat $C(T)$ versus temperature T curve, which suggests the existence of two characteristic energies. We consider that the larger one is J_2 and the other is $(J_1 - J_3)^2/2J_2$ which appears in equation (6).

Acknowledgments

We would like to express our appreciation to H Kikuchi for informing us of their experimental results for azurite prior to publication and for invaluable discussions. We are deeply grateful to Y Ajiro for information and useful discussions on $A_3Cu_3(PO_4)_4$ with A = Ca, Sr. We also thank T Hikihara, by whom the DMRG programme employed in this study is coded, and H Nishimori for the numerical diagonalization program package TITPACK Ver.2. Thanks are further due to H-J Mikeska, K Takano, K Kubo, H Tanaka, H Ohta, K Nomura, A Kitazawa and A Honecker for stimulating discussions. This work has been partly supported by a Grant-in-Aid for Scientific Research on Priority Areas (B) ('Field-Induced New Quantum Phenomena in Magnetic Systems') and a Grant-in-Aid for Scientific Research (C) (no. 14540329) from the Ministry of Education, Culture, Sports, Science and Technology of Japan. Finally, we thank the Supercomputer Center, Institute for Solid State Physics, University of Tokyo, the

Information Synergy Center, Tohoku University and the Computer Room, Yukawa Institute for Theoretical Physics, Kyoto University for computational facilities.

References

[1] Ishii M, Tanaka H, Mori M, Uekusa H, Ohashi Y, Tatani K, Narumi Y and Kindo K 2000 *J. Phys. Soc. Japan* **69** 340
[2] Okamoto K, Tonegawa T, Takahashi Y and Kaburagi M 1999 *J. Phys.: Condens. Matter* **11** 10485
[3] Takano K, Kubo K and Sakamoto H 1996 *J. Phys.: Condens. Matter* **8** 6405
[4] Tonegawa T, Okamoto K, Hikihara T, Takahashi Y and Kaburagi M 2000 *J. Phys. Soc. Japan* **69** (Suppl. A) 332
[5] Tonegawa T, Okamoto K, Hikihara T, Takahashi Y and Kaburagi M 2001 *J. Phys. Chem. Solids* **62** 125
[6] Sano K and Takano K 2000 *J. Phys. Soc. Japan* **69** 2710
[7] Honecker A and Läuchli A 2001 *Phys. Rev.* B **63** 174407
[8] Fujisawa M, Yamaura J, Tanaka H, Kageyama H, Narumi Y and Kindo K 2003 *J. Phys. Soc. Japan* **72** 694
[9] Drillon M, Coronado E, Belaiche M and Carlin R L 1988 *J. Appl. Phys.* **63** 3551
[10] Drillon M, Belaiche M, Legoll P, Aride J, Boukhari A and Moqine A 1993 *J. Magn. Magn. Mater.* **128** 83
[11] Ajiro Y *et al* 2001 *J. Phys. Soc. Japan* **70** (Suppl. A) 186
[12] Sakurai H, Yoshimura K, Kosuge K, Tsujii N, Abe H, Kitazawa H, Kido G, Michor H and Hilscher G 2002 *J. Phys. Soc. Japan* **71** 1161
[13] Kikuchi H, Fujii Y, Chiba M, Mitsudo S and Idehara T 2003 *Physica* B **329–333** 967
[14] Kamikawa T, Okubo S, Takashi K, Ohta H, Inagaki Y, Kikuchi H, Saito T, Azuma M and Takano M 2003 *Physica* B **329–333** 988
[15] Kikuchi H and Mitsudo S 2002 private communications
[16] Lieb E and Mattis D 1962 *J. Math. Phys.* **3** 749
[17] Totsuka K 1998 *Phys. Rev.* B **57** 3435
[18] Tonegawa T and Harada I 1987 *J. Phys. Soc. Japan* **56** 2153
[19] Okamoto K and Nomura K 1992 *Phys. Lett.* A **169** 433 and references therein
[20] Berezinskii Z L 1971 *Zh. Eksp. Teor. Fiz.* **61** 1144
Berezinskii Z L 1971 *Sov. Phys.—JETP* **34** 610 (Engl. Transl.)
[21] Kosterlitz J M and Thouless D J 1973 *J. Phys. C: Solid State Phys.* **6** 1181
[22] Okamoto K and Kitazawa A 1999 *J. Phys. A: Math. Gen.* **32** 4601
[23] Honecker A 1999 *Phys. Rev.* B **59** 6790
[24] Oshikawa M, Yamanaka M and Affleck I 1997 *Phys. Rev. Lett.* **78** 1984
[25] Okamoto K 1992 *Solid State Commun.* **83** 1098
[26] Okamoto K 2002 *Prog. Theor. Phys.* (Suppl. 145) 113
[27] Nomura K and Kitazawa A 2002 *Proc. French–Japanese Symp. on Quantum Properties of Low-Dimensional Antiferromagnets* ed Y Ajiro and J-P Boucher (Kyushu: Kyushu University Press) (*Preprint* cond-mat/0201072)
[28] Kitazawa A 1997 *J. Phys. A: Math. Gen.* **30** L285
[29] Kitazawa A and Okamoto K 1999 *J. Phys.: Condens. Matter* **11** 9765
[30] Kitazawa A and Okamoto K 2000 *Phys. Rev.* B **62** 940
[31] Sakai T and Okamoto K 2002 *Phys. Rev.* B **65** 214403
[32] White S R 1992 *Phys. Rev. Lett.* **69** 2863
[33] White S R 1993 *Phys. Rev.* B **48** 10345
[34] Nomura K and Okamoto K 1994 *J. Phys. A: Math. Gen.* **27** 5773
[35] Nomura K 1995 *J. Phys. A: Math. Gen.* **28** 5451
[36] Okazaki N, Okamoto K and Sakai T 2000 *J. Phys. Soc. Japan* **69** 2419
[37] Okazaki N, Okamoto K and Sakai T 2001 *J. Phys. Soc. Japan* **70** 636
[38] Nakasu A, Totsuka K, Hasegawa Y, Okamoto K and Sakai T 2001 *J. Phys.: Condens. Matter* **13** 7421
[39] Okamoto K, Okazaki N and Sakai T 2002 *J. Phys. Soc. Japan* **72** (Suppl.) 196
[40] Bonner J C and Fisher M E 1964 *Phys. Rev.* A **135** 640
[41] Zigan F and Schuster H D 1972 *Z. Kristallogr.* **135** 416
[42] Dzyaloshinsky I 1958 *J. Phys. Chem. Solids* **4** 241
[43] Moriya T 1960 *Phys. Rev.* **120** 91